Phase Equilibria in Prototype Nb-Pd-Hf-Al Alloys

A. MISRA, R. BISHOP, G. GHOSH, G.B. OLSON

The phase equilibria in two prototype alloys with nominal compositions 60Nb-20Pd-10Hf-10Al and 40Nb-30Pd-15Hf-15Al (in at. pct) are investigated using scanning electron microscopy and X-ray diffraction. The alloys were heat treated at 1200 °C and 1500 °C for 200 hours each. The phase analysis revealed that the alloys were, for the most part, in the three-phase equilibrium between (Nb), Pd_2HfAl, and Pd_3Hf. The compositions of these three phases along with other observed phases such as PdAl and (α-Hf) provide important data for establishing the Nb-Pd-Hf-Al quaternary phase diagram. A preliminary Nb-Pd-Hf-Al phase diagram, with pertinent tie-tetrahedra, was constructed based on the available composition data. The lattice parameters of (Nb), Pd_2HfAl, Pd_3Hf, and the coefficient of thermal expansion of Pd_2HfAl were measured, and models were developed to predict the composition dependence of the mean atomic volumes/lattice parameters of (Nb) and Pd_2HfAl and the temperature dependence of the lattice parameter of the (Nb) phase. The validity of the models was confirmed by good agreement between predicted and experimental values.

I. INTRODUCTION

THE operating temperature currently limits the efficiency of turbine engines, prompting a great deal of research in an effort to design new high-temperature alloys. Nickel-based superalloys are nearing their operating limit as they approach their melting point, thus triggering the need for new alloys that can operate at around 1300 °C. Ideally, such an alloy should have a substantially higher melting point (or low homologous temperature ($<0.5T_m$) at 1300 °C), and at the operating temperature, it should have high creep strength and high oxidation resistance. For oxidation resistance, the material should be capable of passive oxidation, making it capable of forming a protective oxide scale. The refractory metal niobium has a melting temperature of 2467 °C and also has a low density, thus making it an attractive candidate for replacement of nickel.[1] However, Nb has poor oxidation resistance[2] and only moderate strength at high temperatures.[3]

A systems-based approach[4] is underway to develop a new niobium-based alloy for usable performance at 1300 °C or above. The principles of strengthening in classical γ/γ' Ni-based superalloys[5] is extended to design a Nb-based superalloy strengthened by an ordered bcc aluminide phase. In bcc alloys, such strengthening can be achieved by precipitating either $B2$ or $L2_1$ (Heusler) phase.[6,7] The ordered intermetallic needs to have high thermodynamic stability to promote microstructural stability at high temperatures. Furthermore, to maintain coherency over a long period of time and to obtain a uniform distribution of the precipitates, the lattice mismatch should be very small (preferably <0.1 pct).

Quantum mechanical total energy calculation has been carried out using the full potential–linear muffin–tin orbital (FLMTO) method to obtain the heat of formation of several Heusler compounds at 0 K (with the pure elements as the reference state) and their lattice constants.[8] These are listed in Table I. Based on these calculations, it is seen that the Ni-based intermetallic with the lowest lattice mismatch with bcc Nb and highest stability is Ni_2HfAl. In order to decrease the lattice mismatch even more, the Ni was replaced with Pd, which has the same electronic structure but a larger atomic radius. Quantum mechanical calculations of Pd_2HfAl have been performed[9] using the Full Potential Linearized Augmented Plane Wave (FLAPW) method.[10] The calculations show a decreased lattice mismatch and a reasonably high thermodynamic stability. The cohesive properties of Pd_2HfAl are also listed in Table I.

To assist the modeling of phase stability of relevant multicomponent Nb-based alloys, the phase equilibria in two prototype Nb-Pd-Hf-Al alloys are investigated. The equilibrium microstructure of these alloys established at 1200 °C and 1500 °C are characterized by measuring the compositions of the phases and their lattice parameters. Models are developed to predict the atomic volumes/lattice parameters of the niobium solid solution and the Heusler phase. The model predictions are then tested against the experimental data.

II. EXPERIMENTAL PROCEDURE

Two prototype alloys (numbered 995 and 996) were directionally solidified at the GE Corporate Research and Development Center (Schenectady, NY). The alloys were prepared to have the nominal compositions (in at. pct) of 60Nb-20Pd-10Hf-10Al (alloy 995) and 40Nb-30Pd-15Hf-15Al (alloy 996). The compositions of the alloys were based on a conceptual design with the goal of obtaining a two-phase microstructure containing (Nb) and Pd_2HfAl at 1300 °C. The initial composition designs used the heat of formation data obtained from first principles calculations[14] coupled with the Thermo Tech (Surrey Technology Park, Surrey, UK) thermodynamic database.[15]. The starting materials were pure elements of at least 99.95 pct purity. These were weighed to the desired amounts on a Mettler (Columbus, OH) H80 scale with four decimal place accuracy, with a total mass of about 50 g. The melting chamber was evacuated to 1.33×10^{-2} Pa, and then backfilled 3 times with high-purity argon. The charge

A. MISRA, Graduate Student, G. GHOSH, Research Assistant Professor, and G.B. OLSON, Wilson-Cook Chaired Professor in Engineering Design, are with the Department of Materials Science and Engineering, Northwestern University, Evanston, IL 60208-3108. Contact e-mail: g_ghosh@northwestern.edu R. BISHOP, Consultant, is with McKinsey & Company, Chicago, IL 60603.

Manuscript submitted August 16, 2002.

Table I. Calculated Cohesive Properties for Selected Heusler Phases[8,9]

Compound	a (Calc), nm (at 0 K)	a (Expt), nm (at 298 K)	Lattice Mismatch (with respect to pure Nb at 298 K)	$-\Delta E$ (Formation) (kJ/mol)
Ni_2TiAl	0.587	0.5872[11], 0.5865[12]	11.1 pct	82.71
Ni_2VAl	0.578	0.633[12]	12.4 pct	62.36
Ni_2ZrAl	0.610	0.6123[11,12]	7.59 pct	80.35
Ni_2NbAl	0.600	0.5974[11,12]	9.11 pct	66.83
Ni_2HfAl	0.610	0.6081[11,12]	7.59 pct	91.51
Ni_2TaAl	0.595	0.5949[11]	9.86 pct	75.89
Pd_2HfAl	0.634	0.6367[13]	3.96 pct	77.69

Table II. Tracer Diffusion Distances of Elements in bcc Nb Matrix

Element	Diffusion Distance at 1200 °C in 200 h (μm)	Diffusion distance at 1500 °C in 200 h (μm)
Nb	0.5	8.0
Pd	27.8	284.8
Hf	2.0	25.3
Al	4.3	83.1

was then melted by cold crucible induction levitation melting.[16] A Nb seed crystal attached to a water-cooled pulling rod was then lowered into the melt. However, despite a variety of withdrawal rates and rotation speeds, only 5 g of a Hf-Al–rich crystal was pulled from the first alloy (995) and no crystal could be pulled from the second alloy (996). As a result, the alloys created in this manner were not directionally solidified, but only cold crucible induction melted. The compositions turned out to be unintentionally nonuniform, but this allowed us to survey a wider range of phase relations, as will be discussed further in Section III–A.

Samples were cut from the ingots and were then heat treated at 1200 °C and 1500 °C for 200 hours each. Samples for the 1200 °C heat treatment were vacuum encapsulated in a quartz tube with tantalum foil to getter residual oxygen. The 1500 °C heat treatment was performed at the University of Wisconsin at Madison in a high-purity argon atmosphere furnace.

For equilibrium to be attained, the heat treatment period should be sufficiently long to enable the elements involved to diffuse over lengthscales comparable to the microstructural features. The tracer diffusivities (D) of Al and Nb in bcc Nb are known,[17] but those of Pd and Hf in bcc Nb are not known. As an approximation, we treat the tracer diffusivities of Pd and Hf in bcc Nb to be the same as Ni and Zr in bcc Nb, respectively, which have been reported in the literature.[17] Resulting estimates of the tracer diffusion distances ($\approx \sqrt{Dt}$) of each of these elements in bcc Nb at 1200 °C and at 1500 °C in 200 hours are listed in Table II.

Most of the features that are observed in the microstructures (Section III–A) are of the order of 1 to 40 μm. Based on the estimated distances in Table II, we conclude that the 1500 °C samples are very likely at equilibrium, and the 1200 °C samples should be reasonably near equilibrium.

A 10-g button of Pd_2HfAl was made by arc melting in an inert argon atmosphere, to determine its lattice parameter and the coefficient of thermal expansion. The starting materials used were the same as those used for making the prototype alloys. A computer-controlled MMC metallurgical dilatometer was used to determine the coefficient of thermal expansion of Pd_2HfAl.

A Hitachi 4500 scanning electron microscope (SEM) having a cold field emission gun was used for microstructural characterization. Standards-based composition analysis was carried out on a Hitachi (Hitachi, Ltd., Tokyo, Japan) 3500 SEM having a tungsten filament and fitted with a PGT (Princeton Gamma-Tech, Inc., Princeton, NJ) energy-dispersive spectrometer and PGT-IMIX (Integrated Microanalyzer for Imaging and X-ray) software and ZAF (Z = Atomic number; A = Absorption; F = Fluorescence) parameter database. A 20 kV accelerating voltage was used for both imaging and energy-dispersive X-ray analysis. NIH Image software[18] was used to measure the area fraction of the different phases from the representative micrographs. X-Ray diffraction was performed on a Scintag (Scintag, Inc., Cupertino, CA) XDS 2000 diffractometer with a Cu K_α source. The diffraction patterns were then analyzed using MacDiff[19] software to precisely determine the peak positions, assuming split pseudo-voigt shape of the peaks. Lattice parameter values were obtained from the peak positions, and, in the case of (Nb) and Pd_2HfAl, these were plotted against the Nelson–Riley function[20] in order to obtain precise lattice parameter values. In the case of the hexagonal Pd_3Hf phase, Cohen's method[20] was used to obtain the lattice parameters.

III. RESULTS

A. *Microstructure and Phase Analysis*

Alloy 995 showed the presence of three phases after 1200 °C and 1500 °C heat treatments. The phases are identified as (Nb), Pd_3Hf, and Pd_2HfAl. Representative micrographs are shown in Figures 1(a) and (b). The measured compositions of the phases and lattice parameters are summarized in Table III. As seen in the micrographs, (Nb) has a dendritic shape, implying that it has solidified first. Pd_2HfAl is the interdendritic phase in Figures 1(a) and (b). Pd_3Hf almost always appears at the interface between (Nb) and Pd_2HfAl, suggesting that it is a product of solid-state reaction between (Nb) and Pd_2HfAl at 1200 °C and 1500 °C. However, some isolated particles of Pd_3Hf can also be seen in the micrographs.

Alloy 996, heat treated at 1200 °C, showed considerable compositional inhomogeneity. As mentioned in Section II, this inhomogeneity was not intentional, but was a result of macrosegregation occurring during solidification of the sample after cold crucible induction melting. The nonuniform sample nonetheless yields important data as it gives information about the tie-triangles of different equilibria in the Nb-Pd-Hf-Al quarternary phase diagram. Three 3-phase and one 2-phase region

Table III. Measured Composition of the Phases (in Atomic Percent) and Their Lattice Parameters in Alloy 995

Heat Treatment	Phases	Nb	Pd	Hf	Al	Lattice Parameter (nm)
1200 °C	(Nb)	88.5 ± 1.2	7.9 ± 0.8	1.2 ± 0.4	2.4 ± 0.3	a = 0.32912 ± 0.00022
200 h	Pd_2HfAl	0.2 ± 0.2	57.2 ± 0.5	19.2 ± 0.6	23.4 ± 0.5	a = 0.63159 ± 0.00005
	Pd_3Hf	0.4 ± 0.5	73.5 ± 1.3	24.6 ± 1.1	1.4 ± 0.3	a = 0.56178 ± 0.00030
						c = 0.92019 ± 0.00030
1500 °C	(Nb)	89.0 ± 1.1	7.7 ± 0.5	1.2 ± 0.3	2.1 ± 0.5	a = 0.32944 ± 0.00006
200 h	Pd_2HfAl	0.6 ± 0.4	57.1 ± 0.6	19.6 ± 0.8	22.7 ± 0.5	a = 0.63331 ± 0.00001
	Pd_3Hf	0.6 ± 0.3	75.4 ± 0.3	23.6 ± 0.2	0.4 ± 0.4	a = 0.55653 ± 0.00030
						c = 0.91988 ± 0.00030

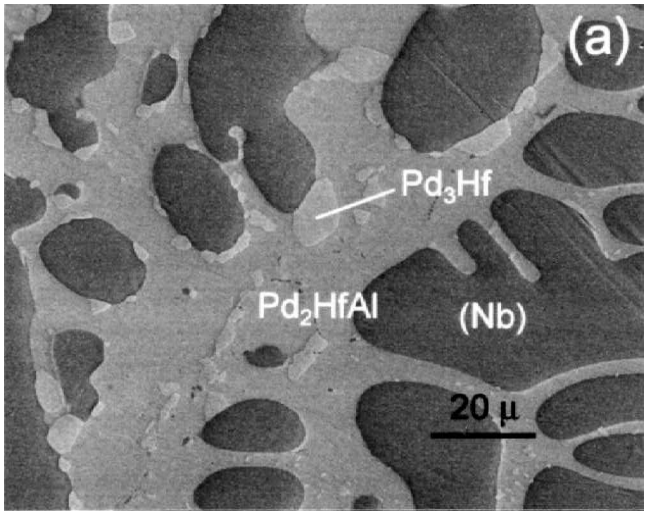

(*a*)

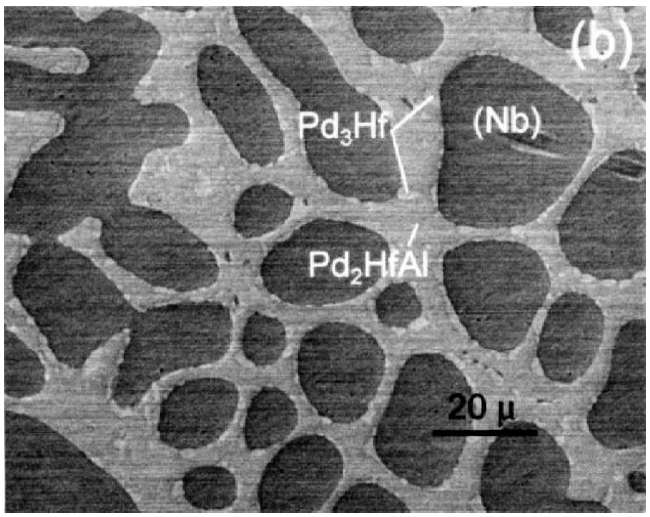

(*b*)

Fig. 1—Microstructure of alloy 995 showing the presence of three phases: (*a*) heat treated at 1200 °C and (*b*) heat treated at 1500 °C.

were observed in the sample. These are (Nb) + (α-Hf) + PdAl (region 1), (Nb) + Pd_2HfAl (region 2), (Nb) + PdAl + Pd_3Hf (region 3), and (Nb) + Pd_2HfAl + Pd_3Hf (region 4). However, the three-phase region of (Nb), PdAl, and (α-Hf) extended over the major part of the sample and the other regions were observed near the edge of the sample. Representative micrographs are shown in Figures 2(a) through (d).

Alloy 996 heat treated at 1500 °C showed the presence of three phases, (Nb), Pd_2HfAl, and a trace amount of Pd_3Hf. However, Pd_3Hf phase in alloy 996 heat treated at 1500 °C was fine and thus it was not possible to perform definitive composition analysis on it in the SEM. Representative micrographs are shown in Figures 3(a) and (b). As can be seen from Figure 3(b), the Pd_3Hf phase appears mainly at the interface between (Nb) and Pd_2HfAl. The compositions of the phases present in alloy 996, along with the lattice parameters for (Nb) and Pd_2HfAl in the alloy heat treated at 1500 °C, are summarized in Table IV.

The Pd_2HfAl alloy was confirmed to be single-phase Heusler by both SEM analysis and X-ray diffraction. The composition of the phase along with the lattice parameter is summarized in Table V.

As a result of the Hf-Al–rich crystal being pulled out from alloy 995 during processing, its actual composition was different from the nominal composition. From SEM observations, it was seen that there was a difference between the relative fractions of the phases at the center region of the sample (where all composition analysis had been carried out) and at the edge of the sample in alloy 995 at both heat treatments. Alloy 996 was obviously inhomogenous, as evident from the presence of four different regions of equilibrium in the sample heat treated at 1200 °C. Due to the preceding considerations, a re-evaluation of the overall compositions of the alloys in the regions of interest was carried out. At least five different low-magnification micrographs from each region were analyzed, and the area fraction of each phase was measured from the micrographs. It was assumed that the apparent area fraction in two-dimensions corresponds to the volume phase fraction in three-dimensions. After rejection of outliers, the values were averaged to obtain the phase fraction at each region. The measured phase fractions are listed in Table VI.

Based on the phase fractions and the composition of each phase, the actual overall compositions of the alloys at the regions of interest were calculated. The calculated overall compositions are listed in Table VII. The listed error bars, related to the uncertainty in the measured compositions (Tables III and IV) and the uncertainty in the measured phase fractions (Table VI), were calculated using a standard mathematical procedure.

B. *A Tentative Phase Diagram for the Nb-Pd-Hf-Al System*

Based on the composition analysis, Nb-Pd-Hf-Al phase tetrahedra were constructed to represent the equilibrium between the observed phases in the four-component system.

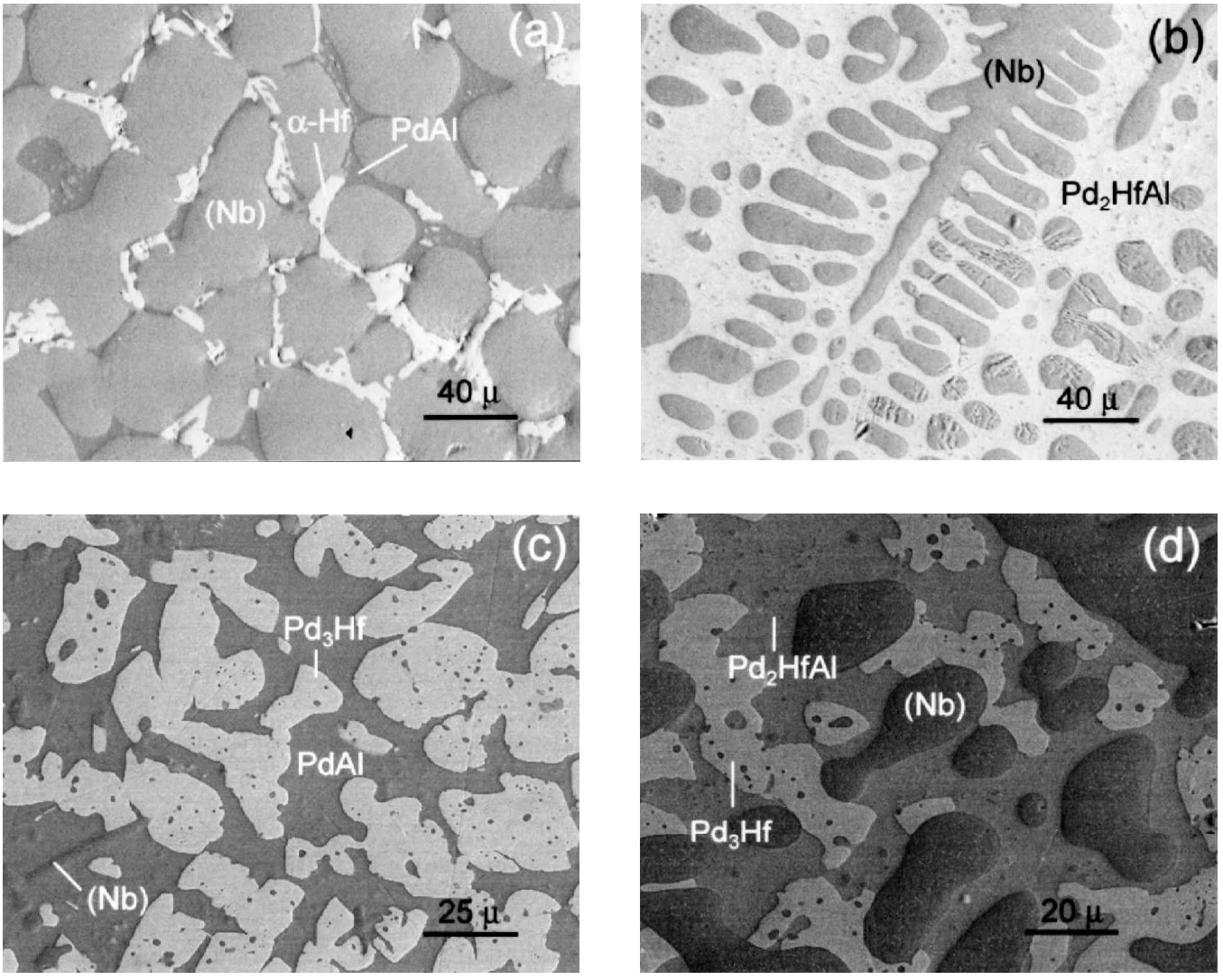

Fig. 2—Microstructure of alloy 996 heat treated at 1200 °C: (*a*) region 1, (*b*) region 2, (*c*) region 3, and (*d*) region 4.

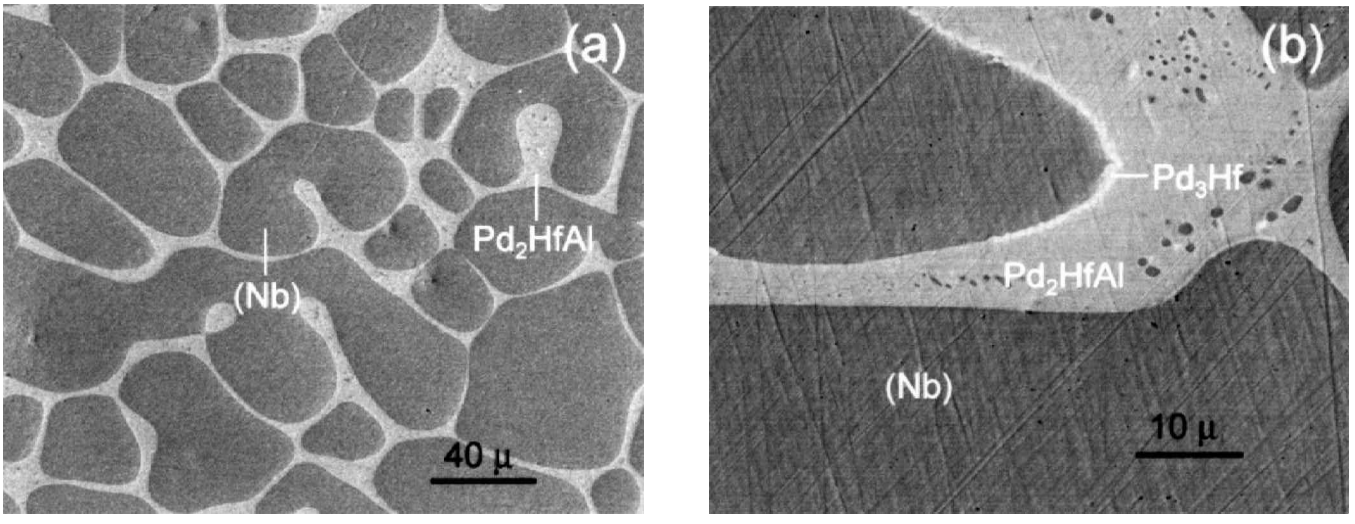

Fig. 3—Microstructure of alloy 996 heat treated at 1500 °C (*a*) at lower magnification showing (Nb) and Pd_2HfAl; and (*b*) at higher magnification showing very fine Pd_3Hf phase, mostly along (Nb)/Pd_2HfAl interface

Table IV. Measured Composition of the Phases (in Atomic Percent) and Their Lattice Parameters in Alloy 996

Heat Treatment	Phases	Nb	Pd	Hf	Al	Lattice Parameter (nm)
1200 °C	Region 1					
200 h	(Nb)	90.7 ± 1.8	3.9 ± 0.8	2.2 ± 1.1	3.2 ± 1.3	—
	PdAl	0.4 ± 0.5	52.5 ± 0.4	0.5 ± 0.2	46.6 ± 0.5	—
	(α-Hf)	0.5 ± 0.9	0.6 ± 0.6	90.7 ± 0.8	8.2 ± 0.6	—
	Region 2					
	(Nb)	90.5 ± 0.9	3.9 ± 0.4	2.0 ± 0.7	3.6 ± 0.4	—
	Pd_2HfAl	0.3 ± 0.2	54.1 ± 2.0	20.7 ± 1.2	24.9 ± 1.2	—
	Region 3					
	(Nb)	90.0 ± 1.3	6.9 ± 0.9	1.0 ± 0.2	2.1 ± 0.5	—
	PdAl	0.2 ± 0.1	55.1 ± 0.4	6.6 ± 0.9	38.1 ± 1.1	—
	Pd_3Hf	0.3 ± 0.3	72.9 ± 0.7	23.2 ± 0.3	3.6 ± 0.5	—
	Region 4					
	(Nb)	92.2 ± 0.9	4.7 ± 0.8	1.2 ± 0.3	1.9 ± 0.5	—
	Pd_2HfAl	0.5 ± 0.4	56.3 ± 0.6	16.0 ± 0.5	27.2 ± 0.4	—
	Pd_3Hf	0.3 ± 0.3	73.2 ± 0.5	23.1 ± 0.4	3.4 ± 0.6	—
1500 °C	(Nb)	89.6 ± 0.8	3.9 ± 0.4	2.1 ± 0.2	4.4 ± 0.4	$a = 0.32962 \pm 0.00005$
	Pd_2HfAl	0.2 ± 0.2	51.6 ± 0.5	22.9 ± 0.3	25.3 ± 0.5	$a = 0.63759 \pm 0.00002$
200 h	Pd_3Hf	—	—	—	—	—

Table V. Measured Composition of Pd_2HfAl (in Atomic Percent) and Its Lattice Parameter in Pd_2HfAl Alloy

Heat Treatment	Phases	Nb	Pd	Hf	Al	Lattice Parameter (nm)
As cast	Pd_2HfAl	0.0	49.6 ± 0.4	25.3 ± 0.3	25.1 ± 0.4	$a = 0.63680$

Table VI. Phase Fractions of Individual Phases

Alloy	Region	(Nb)	Pd_2HfAl	PdAl	Pd_3Hf	(α-Hf)
995 at 1200 °C	central	0.508 ± 0.013	0.423 ± 0.007	—	0.069 ± 0.010	—
995 at 1500 °C	central	0.515 ± 0.026	0.409 ± 0.029	—	0.076 ± 0.011	—
996 at 1200 °C	region 1	0.833 ± 0.027	—	0.064 ± 0.025	—	0.103 ± 0.006
996 at 1200 °C	region 2	0.474 ± 0.031	0.526 ± 0.031	—	—	—
996 at 1200 °C	region 3	0.063 ± 0.025	—	0.345 ± 0.017	0.592 ± 0.008	—
996 at 1200 °C	region 4	0.410 ± 0.105	0.365 ± 0.085	—	0.225 ± 0.043	—
996 at 1500 °C	central	0.863 ± 0.016	0.137 ± 0.016	—	—	—

Table VII. Actual Overall Compositions of Alloy Samples

Alloy	Region	Nb (At. Pct)	Pd (At. Pct)	Hf (At. Pct)	Al (At. Pct)
995 at 1200 °C	central	45.1 ± 1.9	33.3 ± 1.9	10.4 ± 0.9	11.2 ± 0.6
995 at 1500 °C	central	46.2 ± 3.1	33.0 ± 3.2	10.4 ± 1.3	10.4 ± 1.2
996 at 1200 °C	region 1	75.6 ± 4.1	6.7 ± 2.2	11.2 ± 1.6	6.5 ± 2.5
996 at 1200 °C	region 2	43.0 ± 3.4	30.3 ± 3.1	11.9 ± 1.6	14.8 ± 1.7
996 at 1200 °C	region 3	6.0 ± 2.6	62.5 ± 2.3	16.1 ± 0.8	15.4 ± 1.5
996 at 1200 °C	region 4	38.0 ± 10.3	39.0 ± 9.1	11.5 ± 2.9	11.5 ± 3.2
996 at 1500 °C	central	77.3 ± 2.2	10.4 ± 1.3	5.0 ± 0.6	7.3 ± 0.9

Figure 4 shows the various three-phase equilibria present in our alloys heat treated at 1200 °C. We can then proceed to represent an isothermal section of the Nb-Pd-Hf-A1 phase diagram at 1200 °C by projecting the compositions of the Pd_2HfAl phases, the Pd_3Hf phases, the PdAl phases, and the α-Hf phases in equilibrium with bcc Nb on to the Pd-Hf-Al basal plane. This is shown in Figure 5. The phase boundaries represent our best estimate based on available composition data. The solid circles correspond to the projected data points and the open circles represent the reported solubility limits of the binary system.[21,22,23] The Pd_2HfAl data point "A," denoted by a solid square, is based on ongoing research that will be published as part of a future publication.[24] The figures in parentheses indicate the actual Nb content of the phases. The experimental tie-lines are represented by the dashed lines. As seen in Figure 5, the Pd_2HfAl phase tends to be Pd-rich

Figure 5 shows two three-phase regions projected on the Pd-Hf-Al plane. The Nb solid solutions, in equilibrium with those three-phase regions, then define unique tie-tetrahedra in the Nb-Pd-Hf-Al system. This is represented

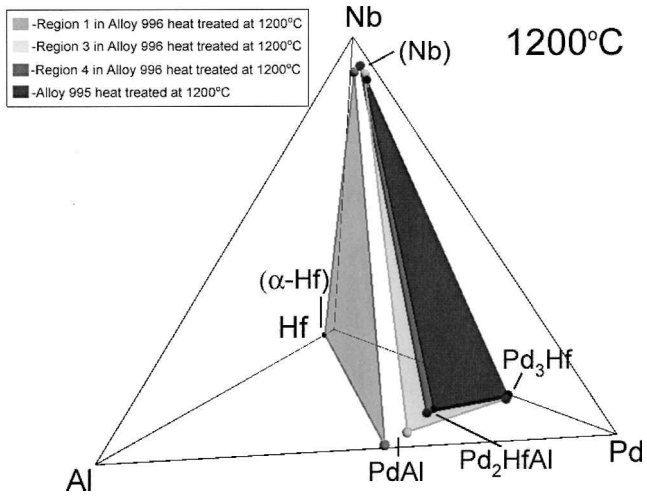

Fig. 4—Experimental tie-triangles in alloys 995 and 996 at 1200 °C.

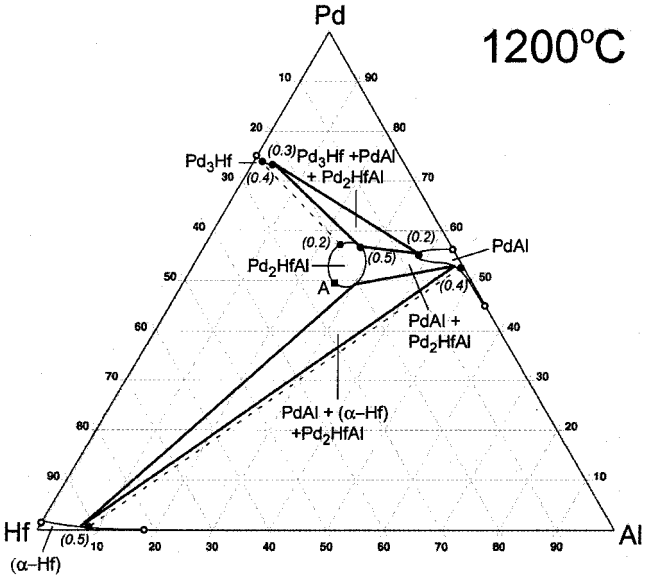

Fig. 5—Projection of Nb-Pd-Hf-Al tie-tetrahedra bases on Pd-Hf-Al plane (1200 °C).

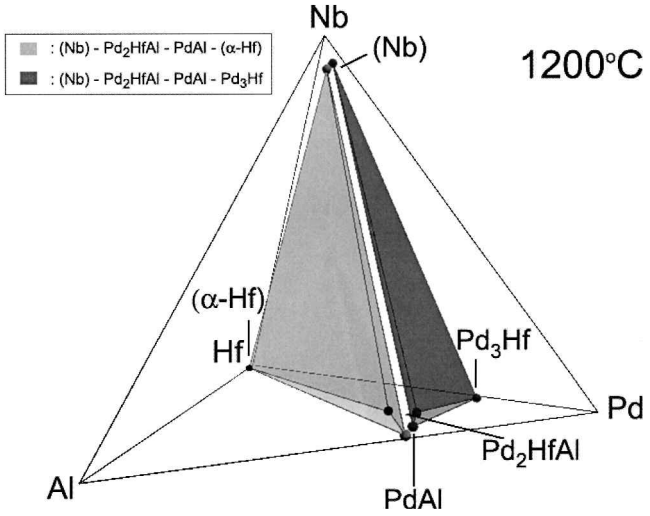

Fig. 6—Tie-tetrahedra in the Nb-Pd-Hf-Al quarternary system at 1200 °C.

in Figure 6. As a preliminary estimate, the composition of (Nb) in the equilibrium tie-tetrahedron (Nb)-Pd_2HfAl-Pd_3Hf-PdAl is taken as the same as that of (Nb) in equilibrium with Pd_2HfAl and Pd_3Hf in region 4 of alloy 996 heat treated at 1200 °C (Table IV). The composition of (Nb) in the equilibrium tie-tetrahedron (Nb)-Pd_2HfAl-PdAl-(α-Hf) is taken as the same as that of (Nb) in equilibrium with PdAl and (α-Hf) in region 1 of alloy 996 heat treated at 1200 °C (Table IV). Any alloy composition within the tie-tetrahedra will result in a four-phase equilibrium with the composition of the phases being given by the corners of the tie-tetrahedra. The separation of the two tie-tetrahedra bases in Figure 6 defines the width of the three-phase fields between them. These three-phase fields in turn define the limits of the desired (Nb)-Pd_2HfAl two-phase field for dispersion-strengthened alloys.

C. *Mean Atomic Volume and Lattice Parameter of Nb-Based Solid Solution and Pd_2HfAl*

To design alloys with controlled misfit between the matrix and the strengthening phase, models are needed to accurately predict the mean atomic volumes/lattice parameters of both phases as a function of composition and temperature. Based on existing literature data, simple analytical functions were derived to express the temperature and composition dependence of the mean atomic volume/lattice parameter of the Nb solid solution and the composition dependence of the lattice parameter of Pd_2HfAl. The coefficient of thermal expansion (CTE) of Pd_2HfAl was measured by dilatometry.

1. *Composition dependence of the mean atomic volume of bcc Nb-based solid solution*

In the spirit of CALPHAD (Calculation of Phase Diagrams) formalism, we present a model to predict the mean atomic volume of bcc Nb with dissolved amounts of Pd, Hf, and Al. In this approach, the composition dependence of the mean atomic volume (or lattice parameter) is expressed using a Redlich–Kister polynomial,[25] which is also used to express the composition dependence of excess Gibbs energy. Then, one advantage is that the effect of misfit strain on phase equilibria can be readily calculated.

The mean atomic volume (V_a) represents half of the volume of the bcc unit cell, as there are two atoms per bcc unit cell. The ambient atomic volume of bcc Nb has been reported by King[26] to be 17.98×10^{-3} nm^3. Literature data reporting the variation of room-temperature lattice parameter of bcc Nb with dissolved amounts of Al[27,28,29] Hf[30,31,32,33] and Pd[34,35] was collected and the data points were converted to mean atomic volumes.

The lattice parameters at 0 K of bcc Al (metastable), bcc Hf, bcc Nb and bcc Pd (metastable), and bcc-based ordered compounds ($B2$ and $B32$ structure with AB stoichiometry and DO_3 structure with A_3B and AB_3 stoichiometry) in the Nb-Pd and Nb-Al systems were calculated[36] using first-principles techniques using the Vienna AbInitio Simulation Package (VASP) package.[37] These values were converted to room-temperature (298 K) values by multiplying each value with a correction factor of 1.00237. The correction factor

was calculated by taking the ratio of the ambient lattice parameter of bcc Nb, as reported by King,[38] over the lattice parameter of bcc Nb at 0 K obtained from first-principles calculations.[36] Before the application of the temperature correction, an initial correction had to be applied to the first-principles calculations of the lattice parameter of bcc Pd and the bcc-based ordered compounds involving Pd. First-principles calculations carried out for fcc Pd at 0 K[36] had resulted in a lattice parameter of 0.39605 nm, which was larger than the value of 0.38783 nm reported by King and Manchester at 25 K.[39] (However, recent FLAPW calculations carried out for fcc Pd have been found to give better results.[9]) This implied that a correction factor of 0.9792 needed to be multiplied with the first-principles value for fcc Pd in order to obtain the value reported in literature. It was assumed that the same correction would apply to the first-principles calculations for bcc-based Pd systems and this correction was applied to bcc Pd and the bcc-based ordered compounds by taking into account the mole fraction of Pd in those compounds. Combining the available experimental lattice parameter data for bcc solid solution, and the lattice parameters of the bcc-based ordered intermetallics obtained by first-principle calculations, the compositional dependence of the ambient mean atomic volume of bcc Nb-Al, Nb-Hf, and Nb-Pd binary solid solutions was expressed as Redlich–Kister polynomials. Even though ordering of a solid solution at the same composition usually results in a slight decrease (~0.5 pct) in lattice parameter (or mean atomic volume), the underlying approximation helps us in expressing composition dependence in the entire composition range.

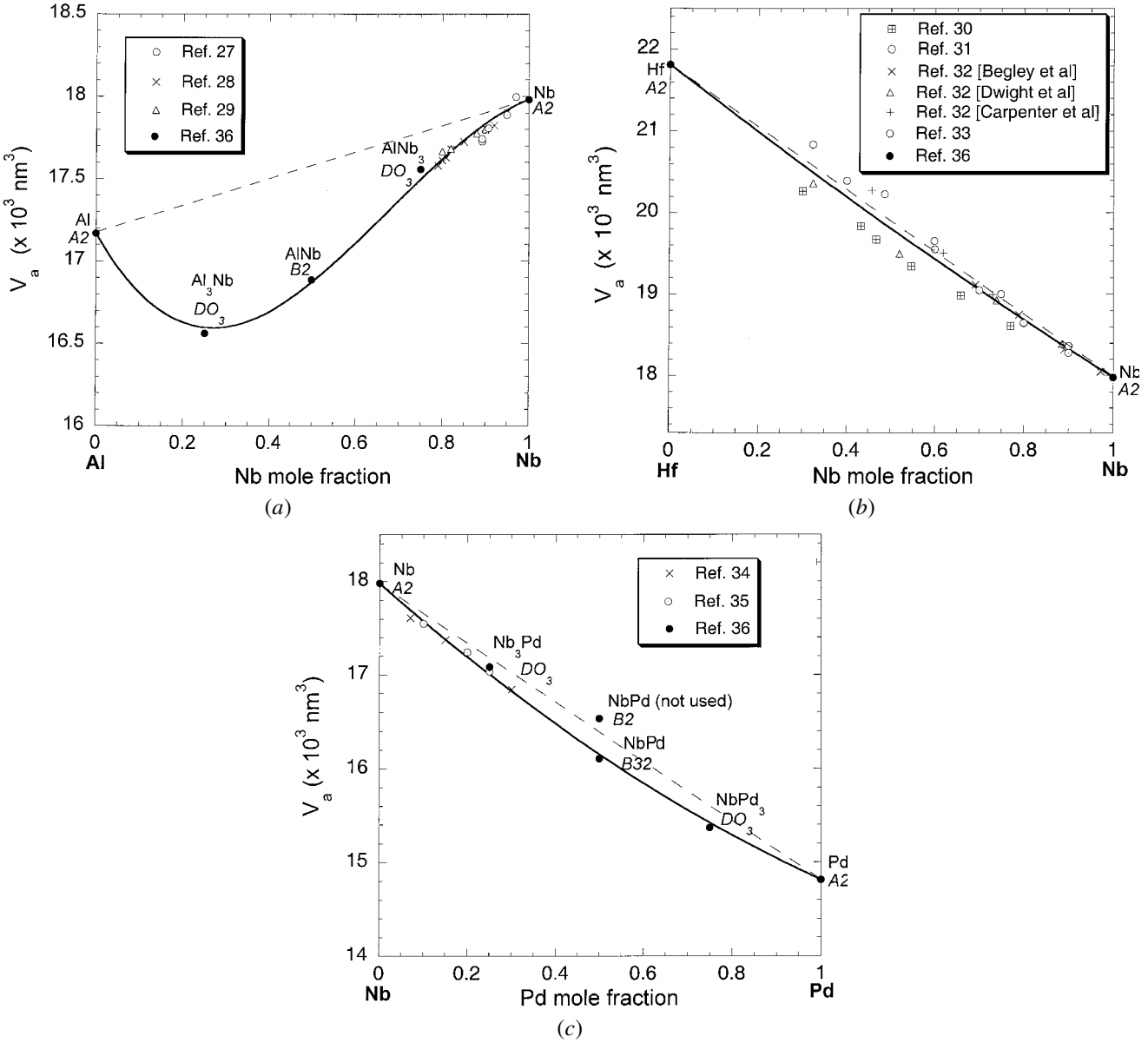

Fig. 7—Variation of mean atomic volume (*a*) of Al-Nb bcc alloys at 298 K showing strong negative deviation from ideal behavior, (*b*) of Hf-Nb bcc alloys at 298 K showing a weak negative deviation from ideal behavior, and (*c*) of Nb-Pd bcc alloys at 298 K showing a moderate negative deviation from ideal behavior.

The composition dependence of the mean atomic volume of bcc Nb-Al, Nb-Hf, and Nb-Pd binary solid solutions is shown in Figures 7(a) through (c), respectively. The following equations represent the compositional variation of the ambient mean atomic volumes of bcc Nb-Al, Nb-Hf, and Nb-Pd binary solid solutions:

$$V_a^{\mathrm{Nb-Al}} \times 10^3\ \mathrm{nm}^3 = 17.169X_{\mathrm{Al}} + 17.980X_{Nb} + X_{\mathrm{Al}}X_{\mathrm{Nb}}\left[-2.8267-2.6218(X_{\mathrm{Al}}-X_{\mathrm{Nb}})\right] \quad [1]$$

$$V_a^{\mathrm{Nb-Hf}} \times 10^3\ \mathrm{nm}^3 = 21.815X_{\mathrm{Hf}} + 17.980X_{Nb} - 0.3573X_{\mathrm{Hf}}X_{\mathrm{Nb}} \quad [2]$$

$$V_a^{\mathrm{Nb-Pd}} \times 10^3\ \mathrm{nm}^3 = 17.980X_{\mathrm{Nb}} + 14.815X_{Pd} - 0.9695X_{\mathrm{Nb}}X_{\mathrm{Pd}} \quad [3]$$

where X_i represents the mole fraction of the corresponding species (i = Nb, Al, Hf, or Pd).

As can be seen from Eqs. [1] through [3], the ambient atomic volumes of bcc Al, Hf, and Pd are 17.169×10^{-3} nm^3, 21.815×10^{-3} nm^3, and 14.815×10^{-3} nm^3, respectively. In Eqs. [1] through [3], the coefficients multiplied by X_iX_j were obtained by least-square fits. The error associated with each coefficient, related to the scatter in the data, is shown in Table VIII.

The linear behavior of the mean atomic volumes for the bcc Nb-Al, Nb-Hf, and Nb-Pd solid solutions are represented by dashed lines in Figs. 7(a) through (c), respectively. As can be seen from Figure 7(a), there is considerable deviation from linearity for the mean atomic volume of the bcc Nb-Al solid solution and hence it is necessary to introduce higher-order terms to account for the nonlinear behavior. The mean atomic volume of the bcc Nb-Pd solid solution also shows a negative deviation from linearity(Figure 7(c)). The variation of the mean atomic volume of the bcc Nb-Hf solid solution shows only a slight negative deviation from linearity (Figure 7(b)). However, as can be seen from Table VIII, the absolute value of the higher-order coefficient in Eq. [2] is much larger than the error associated with the experimental scatter.

Based on the least-square fitting parameters and assuming superposition of Nb-X binary systems, the following Redlich–Kister–Muggianu polynomial[40] is proposed to describe the ambient mean atomic volume of bcc Nb-Al-Hf-Pd solid solution:

Table VIII. Error Associated with Higher-Order Coefficients in Eqs. [1] through [3]

Equation	Higher-Order Term	Coefficient	Error
1	$X_{\mathrm{Al}}X_{\mathrm{Nb}}$	2.8267	0.0744
1	$X_{\mathrm{Al}}X_{\mathrm{Nb}}(X_{\mathrm{Al}} - X_{\mathrm{Nb}})$	2.6218	0.1312
2	$X_{\mathrm{Hf}}X_{\mathrm{Nb}}$	0.3573	0.1764
3	$X_{\mathrm{Nb}}X_{\mathrm{Pd}}$	0.9695	0.0940

$$V_a \times 10^3\ \mathrm{nm}^3 = 17.169X_{\mathrm{Al}} + 21.815X_{\mathrm{Hf}} + 17.980X_{\mathrm{Nb}} + 14.815X_{\mathrm{Pd}} + X_{\mathrm{Al}}X_{\mathrm{Nb}}\left[-2.8267-2.6218(X_{\mathrm{Al}}-X_{\mathrm{Nb}})\right] - 0.3573X_{\mathrm{Hf}}X_{\mathrm{Nb}} - 0.9695X_{\mathrm{Nb}}X_{\mathrm{Pd}} \quad [4]$$

The lattice parameter can be obtained from the mean atomic volume by the relation

$$a\ (\mathrm{nm}) = \sqrt[3]{2V_a} \quad [5]$$

The lattice parameters for the Nb solid solutions in alloys 995 and 996 were calculated by using Eqs. [4] and [5]. The error bars for the predicted lattice parameters, related to the uncertainty of the measured compositions (Tables III and IV), were calculated using a standard mathematical procedure. The measured lattice parameters and the predicted values (using Eqs. [4] and [5]) for the Nb solid solutions (compositions listed in Tables III and IV) are compared in Table IX. Alloy 996 heat treated at 1200 °C was not used for the lattice parameter measurements because of the superposition of several peaks resulting from the different phases present in the sample. As seen in Table IX, the agreement is within 0.4 pct.

2. *Composition dependence of lattice parameter of Pd_2HfAl*

In the following, a model is presented to predict the composition dependence of the lattice parameter of Pd_2HfAl. Our approach is to express the lattice parameter of the Heusler phase ($L2_1$) in terms of the site occupancy and the atomic volume of constituent species. Two important assumptions are made: (1) the atomic volume of a species is independent of the site it occupies and (2) only antisite atoms are considered as constitutional defects in Pd_2HfAl, *i.e.*, no vacancy is present. Then, the volume of the unit cell is the weighted sum of volume of the species. There are three distinct crystallographic sites in a Heusler phase A_2BC where eight A atoms occupy site *I*, four B atoms occupy site *II*, and four C atoms occupy site *III*. In a multicomponent system, these sites may be occupied by one or more atomic species. Knowing the site occupancy of the atomic species j (y_j), either from experiment or from thermodynamic prediction, the lattice parameter may be expressed as

$$a^3 = 8\sum_{j=1}^{n} y_j^I\Omega_j^{L21} + 4\sum_{j-1}^{n} y_j^{II}\Omega_j^{L21} + 4\sum_{j-1}^{n} y_j^{III}\Omega_j^{L21} \quad [6]$$

$$\text{with } \sum y_j^I = \sum y_j^{II} = \sum y_j^{III} = 1\,.$$

where Ω_j is the atomic volume of species j and n is the total number of each species.

At first, the atomic volumes of Pd, Hf and Al in Pd_2HfAl will be determined. For a stoichiometric composition when

Table IX. A Comparison of the Calculated and Experimental Lattice Parameter Results for Bcc Phase in Nb-Pd-Hf-Al Samples

Alloy and Heat Treatment	a (nm), Measured	a (nm), Eqs. [4 and 5]	Difference
Alloy 995 at 1200 °C	0.32912 ± 0.00022	0.32817 ± 0.00013	0.29 pct
Alloy 995 at 1500 °C	0.32944 ± 0.00006	0.32826 ± 0.00009	0.36 pct
Alloy 996 at 1500 °C	0.32962 ± 0.00005	0.32921 ± 0.00009	0.12 pct

$x_{Pd} = 0.50$, $x_{Hf} = 0.25$, $x_A = 0.25$, and $x_{Nb} = 0$, Eq. [6] reduces to

$$a_0^3 = 8\Omega_{Pd} + 4\Omega_{Hf} + 4\Omega_{Al} \quad [7]$$

where a_o is the lattice parameter of stoichiometric Pd_2HfAl.

To express the lattice parameter variation of Pd_2HfAl with varying composition, we follow a method similar to that developed by Kitabjian and Nix[41] for the $B2$ phase and Jung *et al.*[42] for the Heusler phase. In the Pd-rich side of Pd_2HfAl, the volume (V) of a unit cell can be expressed as

$$V = \frac{8}{50}(50 + n^*_{Pd})\Omega_{Pd} + \frac{4}{25}(25 - n^{II*}_{Pd})\Omega_{Hf} + \frac{4}{25}(25 - n^{III*}_{Pd})\Omega_{Al} = a^3 \quad [8]$$

where n^*_{Pd} is the number of antisite defects and

$$n^*_{Pd} = n^{II*}_{Pd} + n^{III*}_{Pd} \quad [9]$$

Also, the atomic fractions of Pd and Hf in Pd_2HfAl can be expressed as

$$x_{Pd} = \frac{(50 + n^*_{Pd})}{100} = \frac{1}{2} + \frac{n^*_{Pd}}{100} \quad [10a]$$

$$\text{and} \quad x_{Hf} = \frac{(25 - n^{II*}_{Pd})}{100} = \frac{1}{4} - \frac{n^{II*}_{Pd}}{100} \quad [10b]$$

Differentiating Eq. [8] with respect to n^*_{Pd} and using Eq. [9], we obtain

$$3a^2\frac{da}{dn^*_{Pd}} = \frac{8}{50}\Omega_{Pd} - \frac{4}{25}\frac{dn^{II*}_{Pd}}{dn^*_{Pd}}\Omega_{Hf} - \frac{4}{25}\left(1 - \frac{dn^{II*}_{Pd}}{dn^*_{Pd}}\right)\Omega_{Al} \approx 3a_o^2\frac{da}{dn^*_{Pd}} \quad [11]$$

Differentiating Eqs. [10a] and [10b], we obtain

$$dn^*_{Pd} = 100dx_{Pd} \quad [12a]$$

$$\text{and} \quad dn^{II*}_{Pd} = -100dx_{Hf} \quad [12b]$$

Combining Eqs. [11] and [12], we obtain

$$\frac{3a_o^2}{16}\left(\frac{da}{dx_{Pd}}\right) = \Omega_{Pd} + \left(\frac{dx_{Hf}}{dx_{Pd}}\right)\Omega_{Hf} - \left(1 + \frac{dx_{Hf}}{dx_{Pd}}\right)\Omega_{Al} \quad [13a]$$

$$\text{or} \quad \frac{3a_o^2}{16}\left(\frac{da}{dx_{Pd}}\right) = \Omega_{Pd} + \left(\frac{dx_{Hf}}{da} \times \frac{da}{dx_{Pd}}\right)\Omega_{Hf} - \left(1 + \frac{dx_{Hf}}{da} \times \frac{da}{dx_{Pd}}\right)\Omega_{Al} \quad [13b]$$

So we have two equations (Eqs. [7] and [13b]) for the atomic volumes and three unknowns (Ω_{Pd}, Ω_{Hf}, Ω_{Al}). Also, there is no reported lattice parameter data of Pd_2HfAl as a function of composition and thus further approximations are needed. As a first approximation, the atomic volumes of Hf and Al in Pd_2HfAl are assumed to be the same as in the $B2$ compounds PdHf and PdAl, respectively. The atomic volume of Pd in Pd_2HfAl is assumed to be the mean of the atomic volumes of Pd in $B2$ PdHf and $B2$ PdAl. This assumption has some physical basis, because in $L2_1$ Pd_2HfAl, both the Hf atoms and the Al atoms have Pd atoms as their nearest neighbors. So, the atomic volumes of Hf and Al in Pd_2HfAl are most likely to be influenced by the interaction of those atoms with Pd atoms. The Pd atoms, however, have 4 Hf atoms and 4 Al atoms as their nearest neighbors. So, the atomic volume of Pd in Pd_2HfAl is going to be equally influenced by Pd-Hf and Pd-Al interactions. The problem now reduces to finding the atomic volumes of the constituent species in $B2$ PdAl and $B2$ PdHf.

Literature data of lattice parameter variation of $B2$ PdAl with composition[43,44] was analyzed, and least-square linear fits to the data were carried out on the Al-rich side and the Pd-rich side of stoichiometry. The nature of the variation suggests the following defect chemistry: (1) on the Pd-rich side, the Pd atoms substitute Al atoms on the Al sublattice; and (2) on the Al-rich side, vacancies reside on the Pd sublattice.[43] Thus, on the Pd-rich side, only the atomic volumes of Pd and Al are involved and the atomic volume of the vacancies need not be considered. So, by considering the Pd-rich side, one can minimize the number of unknown variables. By using the experimental lattice parameter data of B2 PdAl, the atomic volumes of Pd and Al in $B2$ PdAl were obtained using a method developed by Kitabjian and Nix.[41] The following equations used were:

$$\Omega^{PdAl}_{Pd} = \frac{a_o^3}{2} + \frac{3a_o^2}{4}\left(\frac{da}{dX_{Pd}}\right) \quad [14]$$

$$\Omega^{PdAl}_{Al} = \frac{a_o^3}{2} - \frac{3a_o^2}{4}\left(\frac{da}{dX_{Pd}}\right) \quad [15]$$

The slope of the a *vs* X_{Pd} plot on the Pd-rich side $\left(\frac{da}{dX_{Pd}}\right)$ was obtained as -5.8×10^{-04} nm per mole fraction Pd, and the lattice parameter of stoichiometric PdAl (a_o) was taken to be 0.30532 nm. Then, we obtained $\Omega^{PdAl}_{Pd} = 0.014191\,nm^3$ and $\Omega^{PdAl}_{Al} = 0.014272\,nm^3$.

Although the formation of PdHf has been established, its structure has not been determined. Based on related systems, it is likely that PdHf has the CsCl structure at higher temperature.[21] In the absence of any experimental data for $B2$ PdHf, we have used an alternative approach to estimate the atomic volumes of Pd and Hf in hypothetical $B2$ PdHf. Ghosh and Asta[36] have calculated the lattice parameters of bcc-type ordered compounds at 0 K in the Pd-Hf system. The lattice parameter of $B2$ PdHf was calculated[36] to be 0.33149 nm at 0 K. By applying the correction for Pd and the correction for temperature as described in Section III–C–1, the lattice parameter of $B2$ PdHf was obtained to be 0.32883 nm at 298 K. Assuming that there are no vacancies present in the system and complete substitution takes place on either side of stoichiometry, the variation of the lattice parameter of ordered PdHf will be essentially a straight line. We approximate the slope of that line to be equal to the slope of a

straight line joining the lattice parameters of bcc Pd and bcc Hf. With the preceding approximation, the slope of the curve $\left(\frac{da}{dx_{Hf}}\right)$ was obtained to be 4.26×10^{-02} nm per mole fraction Hf. Using the preceding values and Kitabjian's method,[41] the atomic volumes of Pd and Hf in *B*2 PdHf were estimated to be $\Omega_{Pd}^{PdHf} = 0.014323\,nm^3$ and $\Omega_{Hf}^{PdHf} = 0.021233\,nm^3$.

Literature data suggest that in *B*2 transition metal aluminides, there is a large reduction in the atomic volume of Al but only a small reduction in the atomic volume of the transition metals.[41] Based on this trend and also noting that the amount of Nb in Pd_2HfAl in our samples is small, we take the atomic volume of Nb in Pd_2HfAl to be the same as the atomic volume of pure Nb.

Taking $\Omega_{Pd} = 0.014257\,nm^3$, $\Omega_{Hf} = 0.021233\,nm^3$, and $\Omega_{Al} = 0.014272\,nm^3$, and by using Eq. [6], the lattice parameters for the observed Pd_2HfAl compositions (listed in Tables III, IV, and V) were calculated. However, it is found that our model consistently underestimates the lattice parameter compared to the measured values. This implies that there is a systematic error in the model parameters. Thus, further refinement of the model is necessary.

Due to the lack of reported lattice parameter data of Pd_2HfAl as a function of composition, we make use of the measured lattice parameter data of Pd-rich Pd_2HfAl phase (compositions listed in Tables III and IV) and also the lattice parameter of stoichiometric Pd_2HfAl[13] to further refine the model parameters. In order to reduce the number of unknown variables, the Nb contribution to the Pd_2HfAl lattice parameters was ignored. It is important to note that the compositions of the observed Pd_2HfAl phases correspond to approximately constant Al and differ mainly in Hf and Pd contents. Thus, we assume that the observed variation in the lattice parameter is mainly due to the variation of Pd and Hf. In order to further reduce the number of unknown variables, the atomic volume of Al in Pd_2HfAl was taken to be the same as the atomic volume of Al in PdAl. Thus, we have two unknowns (Ω_{Pd} and Ω_{Hf}) and two equations (Eqs. [7] and [13b]). The slopes $\frac{da}{dx_{Pd}}$ and $\frac{da}{dx_{Hf}}$ in Eq. [13b] can be evaluated by plotting the observed Pd_2HfAl lattice parameters as a function of Pd composition and as a function of Hf composition, respectively. By using this method, the slopes are obtained to be $\frac{da}{dx_{Pd}} = -0.0599$ nm per mole fraction Pd and $\frac{da}{dx_{Hf}} = 0.0777$ nm per mole fraction Hf. Equations [7] and [13b] are then solved for Ω_{Pd} and Ω_{Hf}, by using the preceding values and by taking $a_o = 0.6367$ nm. Then, we obtain $\Omega_{Pd} = 0.014737\,nm^3$ and $\Omega_{Hf} = 0.020780\,nm^3$.

As previously done, we take the atomic volume of Nb in Pd_2HfAl to be the same as the atomic volume of pure Nb.

The atomic volumes of the different components used in this model and their atomic volumes in their pure state are summarized in Table X.

The lattice parameter of different compositions of the Heusler phase (compositions listed in Tables III, IV, and V) was then calculated by using the preceding atomic volumes and by using the site occupancy relations. The error bars for the predicted lattice parameters, related to the uncertainty of the measured compositions, were obtained using a standard mathematical procedure. The measured lattice parameters and the predicted lattice parameters of the Heusler phase present in the different samples are summarized in Table XI.

3. *Temperature Dependence of lattice parameter of bcc Nb*

Several authors have reported the room-temperature lattice parameter of bcc Nb[38,45,46] as well as the temperature dependence.[34,36,45,47–49] The ambient lattice parameter (0.33007 nm), as reported by King,[38] is more consistent with the high-temperature and low-temperature lattice parameter values as opposed to the value reported by Roberge[45] (0.33063 nm). Overall, the low-temperature lattice parameter values reported

Table X. A Comparison of the Atomic Volumes of Constituents in Pd_2HfAl, in Metastable Bcc State, and in the Stable Standard State

Element	Atomic Volume in Pd_2HfAl (nm^3) at 298 K	Atomic Volume in Bcc form[36] (nm^3) at 298 K	Atomic Volume in Standard Element Reference[25] (nm^3) at 298 K
Pd	0.014737	0.014815	0.014717 (fcc)
Hf	0.020780	0.021815	0.022321 (hcp)
Al	0.014272	0.017169	0.016603 (fcc)
Nb	0.017980	0.017980	0.017980 (bcc)

Table XI. A Comparison of the Calculated and Experimental Lattice Parameters for Pd_2HfAl

Alloy and Heat Treatment	Pd_2HfAl Composition (At. Pct) Nb	Pd	Hf	Al	*a* (nm), Measured	*a* (nm), Eq. [6]	Difference, Pct
Pd_2HfAl alloy	0.0 ± 0.0	49.6 ± 0.4	25.3 ± 0.3	25.1 ± 0.4	0.63680	0.63693 ± 0.0002	−0.02
Alloy 995 at 1200 °C	0.2 ± 0.2	57.2 ± 0.5	19.2 ± 0.6	23.4 ± 0.5	0.63159 ± 0.00005	0.63226 ± 0.0005	−0.11
Alloy 995 at 1500 °C	0.6 ± 0.4	57.1 ± 0.6	19.6 ± 0.8	22.7 ± 0.5	0.63331 ± 0.00001	0.63280 ± 0.0007	0.08
Alloy 996 at 1500 °C	0.2 ± 0.2	51.6 ± 0.5	22.9 ± 0.3	25.3 ± 0.5	0.63759 ± 0.00002	0.63507 ± 0.0008	0.39

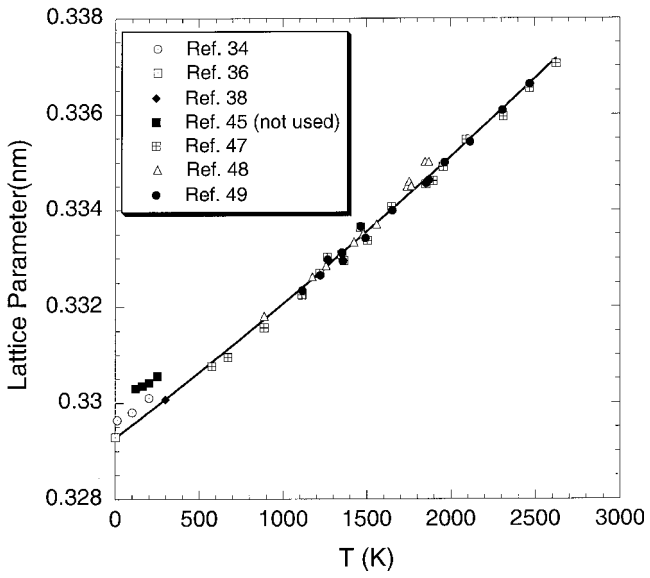

Fig. 8—Variation of lattice parameter of bcc Nb with temperature.

by Roberge[45] are not consistent with other literature data and were not used for the analysis. Taking the room-temperature value of the Nb lattice parameter to be 0.33007 nm, a least-square fit to the literature data yields the following relation:

$$a_{\mathrm{Nb}}(\mathrm{nm}) = 0.33007\left[1 + 8.2987 \times 10^{-6}(T-298) + 3.9363 \times 10^{-10}(T-298)^2\right] \quad [16]$$

Figure 8 shows the variation of the lattice parameter of Nb with temperature. The temperature dependence of the Nb-based solid solution in our system is approximated to be the same as that of pure Nb.

4. *Temperature dependence of lattice parameter of Pd_2HfAl*

X-ray diffraction analysis on the Pd_2HfAl sample revealed the existence of only Heusler phase. The measured lattice parameter has been reported in Table V. Dilatometry tests were carried out on the Pd_2HfAl sample to determine the CTE. The CTE as measured is 8.63×10^{-6}/K for Pd_2HfAl. Thus, the variation of the lattice parameter of stoichiometric Pd_2HfAl with temperature can be expressed as

$$a_{\mathrm{Pd_2HfAl}}(\mathrm{nm}) = 0.6367\left[1 + 8.63 \times 10^{-6}(T-298)\right] \quad [17]$$

D. *Lattice Misfit at 1300 °C*

To determine the unconstrained lattice misfit at an operating temperature of 1300 °C, we use the relation

$$\text{misfit (pct)} = \left(\frac{2a_{\mathrm{Nb}} - a_{\mathrm{Pd_2HfAl}}}{2a_{\mathrm{Nb}}}\right) \times 100 \quad [18]$$

We use Eqs. [16] and [17] to calculate the lattice parameters of (Nb) and the Heusler phase at 1300 °C. The compositions of the Nb solid solution and the Heusler phase are taken to be the same as that in alloy 996 heat treated at 1500 °C (Table IV). The lattice parameters of the Nb solid solution and the Heusler phase and the corresponding misfits at room temperature and 1300 °C are shown in Table XII.

Table XII. Calculated Lattice Misfits between (Nb) and Pd_2HfAl (Listed in Table IV) at 25 °C and 1300 °C

T (°C)	Lattice Parameter of (Nb) (nm)	Lattice Parameter of Pd_2HfAl (nm)	Misfit (Pct)
25	0.32962	0.63759	3.28
1300	0.33331	0.64461	3.30

Thus, the lattice misfit between (Nb) and Pd_2HfAl is approximately the same at the operating temperature as it is at the room temperature. This implies that the only way to reduce the lattice misfit is by the addition of alloying elements, such that the lattice parameter of (Nb) is decreased while that of the Heusler phase is increased. This also requires knowledge of the partitioning behavior of various elements in these two phases as a function of temperature and composition.

IV. CONCLUSIONS

Based on our microstructural characterization and lattice parameter analysis, the following conclusions are drawn.

1. Alloys 995 and 996 were, for the most part, in the three-phase equilibrium between (Nb), Pd_3Hf, and Pd_2HfAl. Three-phase equilibrium was also observed between (Nb), PdAl, and (α-Hf) and (Nb), Pd_3Hf, and PdAl.
2. Two tie-tetrahedra were identified in the Nb-Pd-Hf-Al quarternary system at 1200 °C defining limits of the desired (Nb)-Pd_2HfAl two-phase field.
3. A model is developed and tested to predict the composition dependence of the mean atomic volume and hence the lattice parameter of Nb solid solution with dissolved amounts of Pd, Hf, and Al.
4. A model is developed and tested to predict the composition dependence of the lattice parameter of Pd_2HfAl. This model is based on the site occupancy and atomic volume of constituent species.
5. A model based on least-square fit to literature data was developed to predict the temperature dependence of the lattice parameter of the bcc Nb solid solution.
6. The CTE of Pd_2HfAl was measured by dilatometry tests. The CTE of Pd_2HfAl suggests that its CTE is almost the same as that of Nb at higher temperatures, and as a result, the lattice misfit will remain independent of temperature.

ACKNOWLEDGMENTS

This work was financially supported by the AFOSR-MEANS Program (F49620-01-1-0529) and Reference Metals Company, Inc. We also thank Professor John Perepezko, University of Wisconsin, Madison, for help in heat treating the alloys at 1500 °C.

REFERENCES

1. E.A. Brandes and G.B. Brook: *Smithells Metals Reference Book*, 7th ed., Butterworth-Heinemann, Jordan Hill, Oxford, UK, 1992, p. 2.
2. C. Bouillet, D. Ciosmak, M. Lallemant, C. Laruelle, and J.J. Heizmann: *Solid State Ionics*, 1997, vol. 101, pp. 819-24.
3. M.J. Davidson, M. Biberger, and A.K. Mukherjee: *Scripta Metall. Mater.*, 1992, vol. 27, pp. 1829-34.
4. G.B. Olson: *Science*, 1997, vol. 277, pp. 1237-42.

5. E. Nembach and G. Neite: *Progr. Mater. Sci*., 1985, vol. 29, pp. 177-319.
6. Y. Koizumi, Y. Ro, S. Nakazawa, and H. Harada: *Mater. Sci. Eng. A—Struct*., 1997, vol. 223, pp. 36-41.
7. K. Oh-ishi, Z. Horita, and M. Nemoto: *Mater. Sci. Eng. A—Struct*., 1997, vol. 240, pp. 472-78.
8. W. Lin and A.J. Freeman: *Phys. Rev. B*, 1992, vol. 45, pp. 61-68.
9. A.J. Freeman and M. Kim: Northwestern University, Evanston, IL, unpublished research, 2002.
10. E. Wimmer, H. Krakauer, M. Weinert, and A.J. Freeman: *Phys. Rev. B*, 1981, vol. 24, pp. 864-75.
11. J.H. Westbrook: *Intermetallic Compounds*, John-Wiley & Sons, New York, NY, 1967, p. 174.
12. P. Villars and L.D. Calvert: *Pearson's Handbook of Crystallographic Data for Intermetallic Phases*, ASM INTERNATIONAL, Materials Park, OH, 1991, vol. 1, pp. 877-968.
13. R. Marazza, G. Rambaldi, and R. Ferro: *Atti Della Accademia Nazioonale Dei Lincie*, Classe Di Scienze Fiiche, Matematiche E Naturali, Rendiconti, 1973, vol. 55, pp. 518-21.
14. A.J. Freeman and S.J. Youn: Northwestern University, Evanston, IL, unpublished research, 1998.
15. N. Saunders: *Niobium Database*, Thermotech Ltd., Surrey, UK, 1998.
16. A. Gagnoud, J. Etay, and M. Garnier: *Trans. Iron Steel Inst. Jpn*., 1988, vol. 28, pp. 36-40.
17. E.A. Brandes and G.B. Brook: *Smithells Metals Reference Book*, 7th ed., Butterworth-Heinemann, Jordan Hill, Oxford, UK, 1992, pp. 9-23.
18. http://rsb.info.nih.gov/nih-image/
19. http://servermac.geologie.uni-frankfurt.de/MacDiff.html
20. B.D. Cullity: *Elements of X-Ray Diffraction*, 2nd ed., Addison-Wesley Pub. Co., Reading, MA, 1978, pp. 350-67.
21. S.N. Tripathi and S.R. Bharadwaj: *J. Phase Equilibrium*, 1995, vol. 16, pp. 527-31.
22. J.L. Murray, A.J. McAlister, and D.J. Kahan: *Binary Alloy Phase Diagrams*, 2nd ed, ASM INTERNATIONAL, Materials Park, OH, 1990, vol. 1, pp. 156-57.
23. A.J. McAlister: *Binary Alloy Phase Diagrams*, 2nd ed, ASM INTERNATIONAL, Materials Park, OH, 1990, vol. 1, pp. 189-92.
24. A. Misra, G. Ghosh, and G.B. Olson: *J. Phase Equilibria*, 2003, in press.
25. O. Redlich and A. Kister: *Ind. Eng. Chem*., 1948, vol. 40, pp. 345-48.
26. H.W. King: *Bull. Alloy Phase Diagrams*, 1982, vol. 2, p. 528.
27. H. Hosoda, T. Tabaru, S. Semboshi, and S. Hanada: *J. Alloys Compounds*, 1998, vol. 281, pp. 268-74.
28. J.L. Jorda, R. Flukiger, and J. Muller: *J. Less-Common Met*., 1980, vol. 75, pp. 227-39.
29. V.N. Svechnikov, B.M. Pan, and B.I. Latiesheva: *Metallofizika*, 1968, vol. 2, pp. 54-61.
30. P. Duwez: *J. Appl. Phys*., 1951, vol. 22, pp. 1174-75.
31. A. Taylor and J. Doyle: *J. Less-Common Met*., 1964, vol. 7, pp. 37-53.
32. R.W. Carpenter, C.T. Liu, and P.G. Mardon: *Metall. Trans*., 1971, vol. 2, pp. 125-31.
33. W.A. Jackson, A.J. Perkins, and R.F. Hehemann: *Metall. Trans*., 1970, vol. 1, pp. 2014-16.
34. C.E. Krill III, J. Li, C.M. Garland, C. Ettl, K. Samwer, W.B. Yelon, and W.L. Johnson: *J. Mater. Res*., 1995, vol. 10, pp. 280-91.
35. B.C. Giessen, N.J. Grant, D.P. Parker, R.C. Manuszewski, and R.M. Waterstrat: *Metall. Trans. A*, 1980, vol. 11A, pp. 709-15.
36. G. Ghosh and M. Asta: Northwestern University, Evanston, IL, unpublished research, 2003.
37. G. Kresse and J. Furthmüler: *Phys. Rev. B*, 1996, vol. 54, pp. 11169-11186.
38. H.W. King: *Bull. Alloy Phase Diagrams*, 1981, vol. 2, pp. 401-02.
39. H.W. King and F.D. Manchester: *J. Phys. F: Met. Phy*., 1978, vol. 8, pp. 15-26.
40. Y.M. Muggianu, M. Gambino, and J.P. Bros: *J. Chim. Phys*., 1975, vol. 72, pp. 83-88.
41. P.H. Kitabjian and W.D. Nix: *Acta Metall*., 1998, vol. 46, pp. 701-10.
42. J. Jung, G. Ghosh, D. Ishiem, and G.B. Olson: *Metall. Mater. Trans. A*, 2003, vol. 34A, pp. 1221-35.
43. M. Ettenberg, K.L. Komarek, and E. Miller: *Metall. Trans*., 1971, vol. 2, pp. 1173-81.
44. L.A. Panteleimov, D.N. Gubieva, N.R. Serebryanaya, V.V. Zubenko, B.A. Pozharskii, and Z.M. Zhikhareva: *Vestnik Moskovskogo Universiteta*, Khimiya, Moscow, Russia, 1972, vol. 27, pp. 70-74.
45. R. Roberge: *J. Less-Common Met*., 1975, vol. 40, pp. 161-64.
46. G.B. Grad and J.J. Pieres, Armando Fernandez Guillermet, G.J. Cuello, R.E. Mayer, and J.R. Granada: *Z. Metallkd*, 1995, vol. 89, pp. 395-400.
47. B.M. Vasyutinskiy, G.N. Kartmasov, Y.M. Smirnov and V.A. Finkel: *Phys. Met. Metallogr*., 1966, vol. 21, pp. 134-35.
48. A. Pialoux, M.L. Joyeux, and G. Cizeron: *J. Less-Common Met*., 1982, vol. 87, pp. 1-19.
49. J.W. Edwards, R. Speiser, and H.L. Johnston: *J. Appl. Phys*., 1951, vol. 22, pp. 424-28.